

Self-assembly of Pd Nanoparticles on Anatase Titanium Dioxide and Their Application in Formic Acid Fuel Cells

Qizhi Dong^{1,*}, Tianwu Yin¹, Hansheng Wan¹, Guiming Zhu², Gang Yu¹ and Cancheng Guo^{1,*}

¹ State Key Laboratory of Chemo/Biosensing and Chemometrics, College of Chemistry and Chemical Engineering, Hunan University, Changsha 410082, PR China

² Xiangyang Vocational and Technical College, Xiangyang 441021, PR China

*E-mail: dqzhnu@163.com

Received: 27 October 2015 / Accepted: 21 November 2015 / Published: 1 December 2015

Based on electrostatic self-assembly technology, Pd electrocatalyst with high efficiency and excellent CO-tolerance, which is supported on TiO₂ surface modified by amino-rich, cationic poly (diallyldimethylammonium chloride) (PDDA), was prepared. Through electrostatic interaction, Pd precursors were uniformly distributed on TiO₂ (P) and then in situ reduced into Pd nanoparticles (NPs). In such process, PDDA produced a large number of amine to facilitate the uniform distribution of Pd NPs on the surface of TiO₂. After that, Pd/TiO₂ (P) was mixed with carbon black as anodic catalysts for formic acid oxidation reaction. Transmission electron microscope images and X-ray diffraction patterns revealed that Pd NPs with an average size of ~3 nm were uniformly dispersed on TiO₂. Moreover, with the application of cyclic voltammetry and chronoamperometry, we demonstrated the significant enhancement in the electrocatalytic activity and the tolerance toward CO poisoning when compared with Pd/TiO₂-C for direct formic acid fuel cells.

Keywords: Palladium; self-assembly; anatase-TiO₂; formic acid fuel cells; electrooxidation

1. INTRODUCTION

Recently, direct formic acid fuel cells (DFAFCs) have gained great attention for its promising application prospect in transportation and portable electronic devices [1-2]. Compared with the direct methanol fuel cell (DMFC), DFAFCs has now been gradually recognized because of its outstanding advantages. As a non-flammable liquid at room temperature, Formic acid is non-toxic when being used in a dilute concentration. Compared with methanol, the lower fuel crossover rate of formic acid is capable of achieving a thinner membrane and a higher fuel concentration possible in DFAFCs [3].

It is well known that formic acid oxidation (FAO) could be processed through a dual-path mechanism: the direct oxidation of formic acid through dehydrogenation (1) and the indirect oxidation of formic acid through dehydration of formic acid (2), which produce an adsorbed CO intermediate [4-5].



Precious metal nano-materials have wide application in catalytic field [6-8]. Pt and Pd based nano-materials are extensively used as anode electrocatalysts to catalyze formic acid oxidation in DFAFCs [9-11]. Under the condition of lower potentials, the Pt catalyst presents a lower activity for FAO because of the accumulation of CO_{ads} on its surface by the indirect route. Comparatively, Pd is a preferable catalyst for FAO due to its promotion effect towards dehydrogenation at lower potentials and as well as relatively stronger resistance to CO_{ads} poisoning. However, Pd shows higher activity towards FAO on account of the dominant direct pathway, but its activity gradually weakens due to the blocking of active sites caused by accumulation of CO-like species. Therefore, in order to improve the catalytic activity and stability of Pd catalyst, much effort has been devoted.

As we all know that the support of metal catalysts plays a vital role in electrocatalysis of fuel cell [12-13]. A fine interaction between the metal and support can not only help to decrease the aggregation of metal NPs and improve the efficiency of catalyst, but also can enhance the catalytic performance and durability of catalyst by eliminating catalyst poison (e.g. CO). With regard to low temperature fuel cells, the carbon black, especially Vulcan XC-72R carbon black, is commonly used to support noble metal catalysts [14]. Nevertheless, carbon is likely to be corroded in the harsh fuel cell environment, leading to the aggregation of Pd NPs and resulting in the deterioration of catalyst performance [15-16].

It is interesting but true that TiO_2 can be evaluated as catalyst support material because of its outstanding mechanical stability and higher corrosion resistance under acidic and oxidative conditions [17-18]. We have confirmed that the Pd/ TiO_2 -C composite catalysts exhibit higher catalytic activity and higher electrochemical stability as compared to Pd/C catalysts, and however, due to the chemical inertness of TiO_2 , Pd is not uniformly distributed on the surface of TiO_2 [19]. Therefore, it is necessary to functionalize the surface of TiO_2 to introduce more active sites before Pd NPs deposition. The non-covalent functionalization achieved by PDDA can lead to a homogeneous distribution and high-density of surface functional groups while preserving the intrinsic properties of the support [20-21].

Herein, the highly dispersed Pd NPs are successfully loaded on the surface of intact TiO_2 through electrostatic self-assembly. Pristine TiO_2 are firstly non-covalently functionalized with the positively charged poly (diallyldimethylammonium chloride) (PDDA), which can provide many uniformly distributed active sites for depositing Pd NPs. As a result, the Pd NPs can be deposited on TiO_2 surface with unchanged integrity of TiO_2 . The whole process is illustrated as figure.1: TiO_2 were firstly wrapped with PDDA to obtain TiO_2 (P); then the negatively charged Pd precursors were adsorbed on the surface of TiO_2 through being electrostatically interacted with the positively charged groups of PDDA; finally, the Pd NPs were in situ reduced and deposited on the surface of TiO_2 . Compared with the Pd/ TiO_2 -C catalyst, the Pd/ TiO_2 (P)-C electrocatalyst proposed in this paper was

demonstrated to be of an improved activity and higher stability towards the electrooxidation of formic acid.

2. EXPERIMENTAL SECTION

For the experimental section, materials such as sulfuric acid (H_2SO_4), formic acid (HCOOH), and hydrochloric acid (HCl), palladium chloride (PdCl_2), sodium borohydride (NaBH_4), trisodium citrate ($\text{Na}_3\text{C}_6\text{H}_5\text{O}_7 \cdot 2\text{H}_2\text{O}$), were all obtained from Sinopharm Chemical Reagent Co., Ltd and can be used directly. All reagents used, unless stated otherwise, were of analytical reagent grade. Anatase- TiO_2 with particle size of 15~20 nm and poly (diallyldimethylammonium chloride) (PDDA, average MW: 100,000–200,000) were obtained from Aladdin Industrial Corporation. XC-72R carbon black ($S_{\text{BET}} = 240 \text{ m}^2 \cdot \text{g}^{-1}$) was purchased from Cabot and processed by refluxing treatment in 5M HNO_3 . Water was always double distilled and deionized before using.

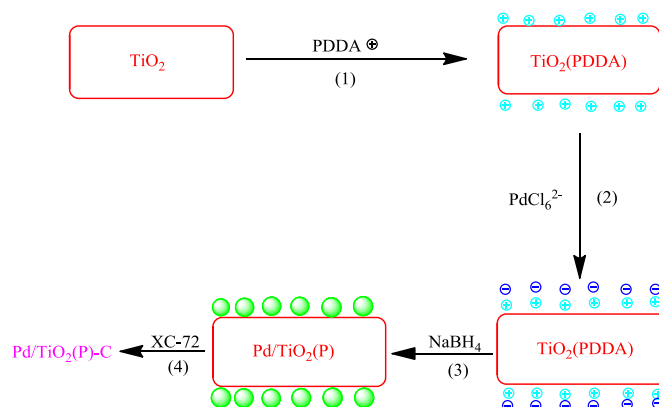


Figure 1. The preparation process of Pd/TiO₂ (P)-C

2.1. Catalysts preparation

For the catalysts preparation of this experiment, the non-covalent functionalization of TiO_2 with PDDA can be described as follows. Firstly, a 500 mg of pristine TiO_2 were dispersed in 500 mL of 0.5 wt.% PDDA aqueous solution, which served as the functionalization polyelectrolyte [22]. Then, keep the solution in ultrasonic treatment for 1 h and being stirred for overnight to guarantee the presence of well-dispersed PDDA. After that, 2 g of NaCl was added to increase the ionic strength of solution, and then increase the attractive force of PDDA towards the TiO_2 surface, thus leading to a higher functionalization degree of polyelectrolyte chains on TiO_2 . It is worth noting that the functionalized TiO_2 should be washed using ultrapure water for several times to remove the excessive PDDA. Finally, the solution was filtrated and dried at 80°C for 10 h in vacuum before obtaining the products noted as TiO_2 (P).

After dropwise addition of a calculated amount of trisodium citrate solution into stirred TiO_2 (P) water slurry, kept stirring the mixture for 1 h. Then, a stoichiometric amount of H_2PdCl_6 solution

(PdCl₂ dissolved in 0.1 M HCl) was added in the mixture, and kept stirring for another hour before dropwise addition of excessive amounts of 0.01 M freshly prepared NaBH₄. Subsequently, the carbon slurry was added into the mixture which was still under continually vigorous stirring. After a further 10 min of stirring, the mixture was filtered and then washed with copious deionized water for enough times in order to guarantee all remaining reducing agents were completely removed. Finally, the resulted solids were dried in vacuum for 24 h at 80 °C. On the other hand, catalysts denoted as Pd/TiO₂ (P)-C. Pd/TiO₂-C were also prepared by similar method as contrast. The preparation process is shown in figure.1.

2.2 Characterization of catalysts

All TEM micrographs of catalysts were obtained on a JEM-3010 transmission electron microscope operated under the condition of 300 kV voltage and 0.17 nm spatial resolution. The samples were ground into fine particles and then fully dispersed in alcohol for ultrasonic treatment. After that, a drop of the dispersion was transferred onto a standard carbon-film-coated copper grid for taking electron micrographs.

XRD patterns of all investigated electrocatalysts were recorded by a SHIMADZU (XRD-6100) diffractometer under Cu K α irradiation at 30 mA and 40 kV. The scan rate was 4 °min⁻¹ and the angular resolution (2θ) of the diffractometer was 0.05 °.

2.3 Preparation for electrodes and electrochemical measurements

The underlying substrate of the working electrode was glassy carbon electrode with 3 mm of diameter and 0.0706 cm² of electrode apparent area. This glassy carbon electrode was polished with successively 0.3 μ m and 0.05 μ m alumina slurry to the extent of mirror finish before using in each experiment. The catalyst was loaded onto the substrate as follows. Under the condition of ultrasonic vibration, the dilute suspension of catalyst was fully dispersed, and then 10 μ L of the dispersed catalyst dilute suspension was dropped onto the surface of polished glassy carbon electrode. After that, 10 μ L of Nafion (5 wt.% dilute solution mixed with ultrapure water and lower aliphatic alcohols) was dropped onto the electrode surface. It is worth noting that the Pd loading on each working electrode was constant as 0.056 mg·cm⁻².

All electrochemical measurements were conducted in a conventional three-electrode system at 25 °C using an Ingsens 3030 electrochemical workstation linked with an SAMSUNG PC. As previously described, the working electrode was prepared. In this experiment, the Pt net (1 cm²) was selected as the counter electrode. All the measured potential values were related to saturated calomel electrode (SCE) in this work. Prior to each measurement, ultrapure argon was kept bubbling into the 0.5 M H₂SO₄ as the electrolyte solution with or without 0.5 M HCOOH for 20 min. The cyclic voltammograms (CV) curves were measured at voltages ranged from - 0.2 V to 1.0 V. Also prior to each measurement, the working electrode was treated with constantly cycling at 50 mV·s⁻¹ with voltages ranged from - 0.2 V to 1.0 V to remove any possible contaminants on Nafion membrane,

until realizing a stable response of working electrode (keep all electrodes processed for the same length of processing time).

3. RESULTS AND DISCUSSION

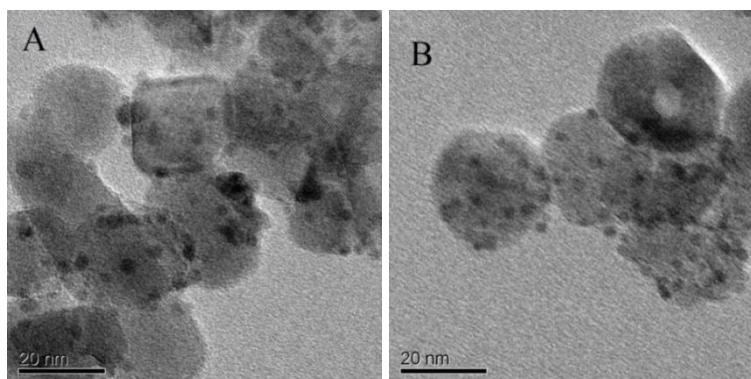


Figure 2. TEM images of the Pd/TiO₂-C (A), Pd/TiO₂ (P)-C (B)

TEM images of Pd/TiO₂-C and Pd/TiO₂ (P)-C are shown in Fig.2. From the TEM image of Pd/TiO₂-C, we can see that Pd was dispersed onto the TiO₂ support in a wide particle size distribution, the agglomeration of Pd particles was found obviously in samples with larger particles, while on some TiO₂ surfaces, there is no distribution of Pd NPs. The causes for such result may be the insufficient amount of active sites on the titanium dioxide surface for the load Pd NPs or may be the uneven distribution of active sites. From the Fig.2B, it can be found that Pd NPs supported on the surface of TiO₂ which have been modified with PDDA are of smaller size than that in the Pd/TiO₂-C catalyst, Pd/TiO₂ (P)-C is of a more narrow particle size distribution, and the Pd NPs on the surface of TiO₂ (P) are in a more uniform and dense distribution.

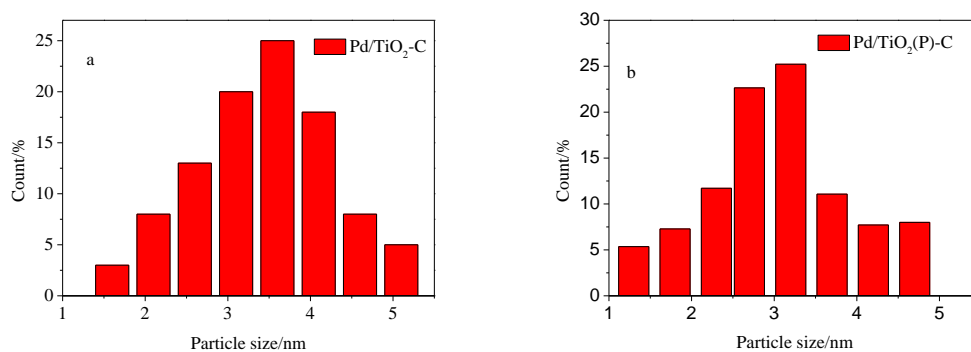


Figure 3. Particle size distribution of Pd NPs in Pd/TiO₂-C and Pd/TiO₂ (P)-C

The average size of Pd NPs in Fig.3 was calculated based on TEM data by averaging the sizes of 50 particles which were randomly selected from the region in Fig.2A and Fig.2B. Through

comparing the average particle sizes between Pd/TiO₂-C (~3.5nm) and Pd/TiO₂(P)-C (~3.0nm), it can confirm that Pd NPs on TiO₂(P) surface were of smaller average particle size than that on untreated TiO₂ surface. Through the electrostatic interaction between the positive nitrogen groups and the Pd NPs precursor, the distribution of the precursor was undoubtedly more homogeneous than the untreated surface of titanium dioxide. Subsequently, a more uniform distribution of Pd NPs was naturally achieved by in-situ reduction.

We believe that this intensive distribution will improve the conductive performance of catalyst in a certain extent, and the uniform distribution of Pd NPs will inhibit the reunion phenomenon in the catalytic process.

The results clearly demonstrate that the wrapping effect of PDDA upon the side walls of TiO₂ can produce a large number of amine in uniform distribution, which then act as anchor sites for the self-assembly of Pd precursors, so that the synthesis of highly dispersed and fine Pd NPs can be achieved. These results demonstrate that PDDA-functionalization is an effective method for enhancing the synthesis of uniformly distributed Pd NPs [23].

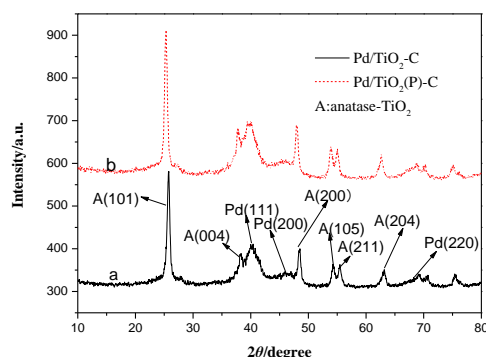


Figure 4. XRD patterns of Pd/TiO₂-C and Pd/TiO₂(P)-C

The XRD patterns of Pd/TiO₂-C catalyst and Pd/TiO₂-C (P) catalyst are shown in Fig.4. The reflection peaks upon $2\theta=40.0^\circ$, 46.5° and 68.1° are derived from the Pd (111) plane, Pd (200) plane and Pd (220) plane in face-centered cubic (fcc) phase, respectively [24]. $2\theta=25.3^\circ$, 37.8° , 48.0° , 53.8° , 54.9° , 62.5° respectively refer to the surface of (101), (004), (200), (105), (211) and (204) planes of anatase titanium dioxide [25]. Due to the existences of strong diffraction peaks of TiO₂, the peak of carbon (002) plane is overlapped by the TiO₂ (101) diffraction peak. Fig.4 illustrates that the crystal structure of TiO₂ remains unchanged after modification. The diffraction peaks at planes from Pd (200) and Pd (220) are also overlapped with other diffraction peaks of anatase TiO₂. Given that the Pd (111) diffraction peak was partially overlapped by the anatase TiO₂ (004) diffraction at $37.8^\circ(2\theta)$, however, the right part of Pd (111) peak was still unaffected. Based on Debye-Scherrer equation [26], the right part of Pd (111) peak was used to calculate the average crystallite size with although a not quite high accuracy. The average crystallite sizes were found to be 4.3 nm for Pd/TiO₂-C and 3.7 nm for Pd/TiO₂(P)-C, respectively. Basically, there is an agreement between the average particle size obtained from TEM study and the average particle size obtained from XRD study. Both TEM and XRD experiments

show that polymer surface modification is of great enhancement to the reduction of the Pd NPs size, electrochemical surface area of catalyst (ECSA) and the utilization rate of Pd will increase with the decrease of the metal catalyst nanoparticle size.

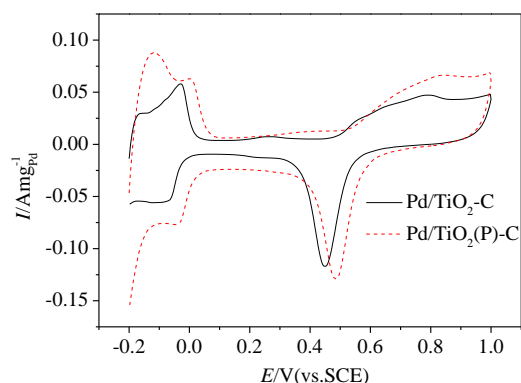


Figure 5. CV curves of the Pd/TiO₂-C and Pd/TiO₂ (P)-C catalysts in a solution of 0.5M H₂SO₄ at a scan rate of 50 mV·s⁻¹.

Fig.5 shows the CV curves of different Pd electrocatalysts scanned at 50 mV·s⁻¹ in 0.5M H₂SO₄ aqueous solution, in which all these electrocatalysts exhibit logical behaviors. Specifically, from the curves, we can clear see the hydrogen adsorption/desorption peaks at - 0.20–0V, the peak of PdO_x formation at higher potentials by forward scan, and the PdO_x reduction peak at 0.35–0.55V by reverse scan. The CV results are in correspondence with the previous report [27-28]. Through calculation, the ECSA of all prepared catalysts were obtained, which then gave an insight into available active sites on catalyst surfaces. Due to the overlap of hydrogen adsorption / desorption peak on Pd surface, and in order to achieve a higher accuracy, the charge consumed in PdO_x reduction during the cathodic scan was taken into account to calculate the ECSA as well as the charge consumed in monolayer oxide reduction was assumed to be 0.424 mC·cm⁻². This method is widely accepted in the literature [29-30]. All these calculated ECSA values are summarized in Table 1, as it can be observed that the Pd/TiO₂ (P)-C achieved relatively higher ECSA values (54.2m²·g⁻¹) over the Pd/TiO₂-C (50.2m²·g⁻¹) did due to the advantages of better dispersion and smaller average particle size of Pd supported on TiO₂ (P). In addition, regarding the peak reduction potential value on the Pd/TiO₂-C catalysts, the reduction peak potential of Pd(OH)₂ on Pd NPs of TiO₂ (P)-C catalyst shifted positively, which indicates the reduced oxophilicity and weakened chemisorption of oxygen-containing species (CO_{ad} and OH_{ad}) on Pd NPs [31].

Table 1. Summary of the electrochemical data of Pd/TiO₂-C and Pd/TiO₂ (P)-C composite catalysts

Sample	ECSA (m ² ·g ⁻¹)	Mass activity (A·mg ⁻¹)	Specific activity (mA·cm ⁻²)	Peak potential (V)
Pd/TiO ₂ -C	50.2	1.32	2.63	0.17
Pd/TiO ₂ (P)-C	54.2	1.54	2.84	0.16

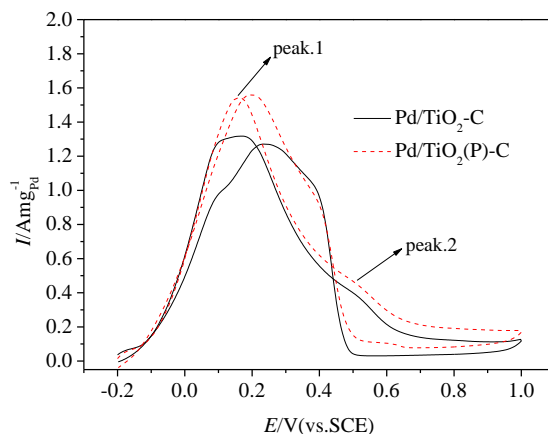


Figure 6. CV curves of formic acid electrooxidation on Pd/TiO₂-C and Pd/TiO₂(P)-C catalysts in a solution of 0.5M H₂SO₄+0.5M HCOOH at a scan rate of 50 mV·s⁻¹.

Fig.6 depicts the CV curves of catalytic electrooxidation of formic acid on Pd/TiO₂-C anode and on Pd/TiO₂(P)-C anode in 0.5 M H₂SO₄ and 0.5M HCOOH, respectively at a sweep speed of 50mV·s⁻¹. As two key parameters in electrocatalysis, the anodic peak current density and peak potential represent the catalytic capability of material for FAOR and the amount of formic acid oxidized on electrocatalyst surface, respectively [32]. During the forward scan, all electrocatalysts show a peak (Peak.1) at low potentials (0–0.3V), which was resulted from the direct oxidation (deprotonation) pathway of HCOOH. Within the potential range of 0.3–0.6V, there is another peak (Peak.2) appearing near Peak.1, which was presumably caused by the additional over-potential for the oxidation of adsorbed CO_{ads} [33-35]. The peak.1 current density of Pd/TiO₂-C during the forward scan is 1.32 A·mg⁻¹ which is lower than that of Pd/TiO₂(P)-C 1.54 A·mg⁻¹.

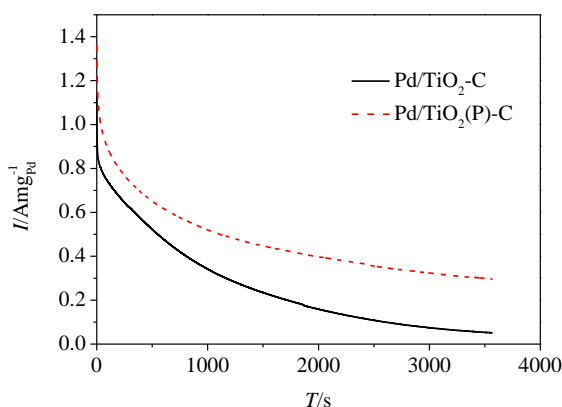


Figure 7. The *i*-*t* curves of formic acid electrooxidation on Pd/TiO₂-C and Pd/TiO₂(P)-C catalysts at 0.1V in a solution of 0.5M H₂SO₄+0.5M HCOOH

Such result may be due to the reduced Pd NPs size in Pd/TiO₂(P)-C, the higher ECSA of Pd unit mass and the increased utilization rate of Pd. The peak potential of anodic oxidation on Pd/TiO₂

(P)-C was shifted negatively by ~10 mV compared to that of Pd/TiO₂-C, which indicates that HCOOH is more susceptible to oxidation on the surface of Pd/TiO₂ (P)-C than to that on the surface of Pd/TiO₂-C [36]. This situation is caused by the decreased adsorption of CO_{ad} on the Pd NPs surface in Pd/TiO₂ (P)-C. Since the specific activity of electrocatalyst is another key parameter to the evaluation of catalytic activity. Table 1 also lists the specific activities of catalysts, which were calculated based on ECSA values and mass activities. As it shows that Pd/TiO₂ (P)-C is also more superior to Pd/C in terms of specific activity.

In order to further compare the catalytic performance and stability between as-prepared Pd/TiO₂-C and Pd/TiO₂ (P)-C, chronoamperometry tests were conducted in aqueous solution of 0.5 M H₂SO₄ and 0.5 M HCOOH at 0.1 V for 3600 s (see Fig.7). The current densities of electro-oxidation for formic acids on the two catalysts vary in a similar way, which is decreasing sharply and then remaining relatively steady, wherein, the decrease tendency reflects catalyst poisoning caused by CO_{ads} chemisorbed on the surface of Pd NPs [37]. As time goes on, the stability of the Pd/TiO₂ (P)-C is found to be better than that of the Pd/TiO₂-C catalyst. In addition, the current density of Pd/TiO₂ (P)-C is larger than the that of Pd/TiO₂-C throughout all the ranges up to 3600 s, revealing advantage of CO-tolerance ability of Pd/TiO₂ (P)-C over Pd/TiO₂-C. After an hour of testing, the current density of Pd/TiO₂-C remains only 5.3% of the initial level, while that of Pd/TiO₂ (P)-C remains still 26.5 % of the initial level. This may be because of the decreased adsorption of CO_{ad} on the Pd NPs surface in Pd/TiO₂ (P)-C, the reduced degree of catalyst poisoning, which improve catalyst stability.

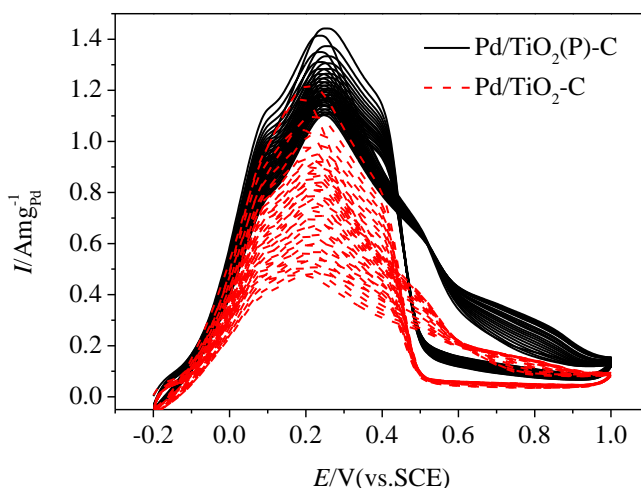


Figure 8. The continuous CV curves of formic acid electrooxidation on Pd/TiO₂-C and Pd/TiO₂ (P)-C catalysts in a solution of 0.5 M H₂SO₄+0.5 M HCOOH at a scan rate of 50 mV·s⁻¹.

To further measure the stability of the catalyst, the continuous cyclic voltammograms test was carried out with 20 test laps. The results are shown in Fig. 8 that current densities of the peak.1 at 20 th circle were 1.10 A·mg⁻¹ and 0.48 A·mg⁻¹, which were reduced by 22.5% and 58.6% respectively from the first circle. Therefore, we can conclude that the stability of Pd/TiO₂ (P)-C is much higher than that of Pd/TiO₂-C.

4. CONCLUSIONS

In this paper, we presented a simple method to synthesize the Pd electrocatalyst of high efficiency and CO-tolerance with the support of PDDA-functionalized TiO₂, and prepared the Pd/TiO₂ (P)-C catalyst. The results showed that noncolvant functionalized TiO₂ by PDDA was capable of providing uniformly distributed and high-density anchoring sites for self-assembly of Pd precursor and without damaging its integrity. Through TEM analysis, we confirmed the possibility of synthesizing the fine Pd NPs which is in uniform distribution and slight aggregation with particle size of around 3.0 nm which supported on the surface of TiO₂ (P). A combined study of cyclic voltammetry and chronoamperometry demonstrated that Pd/TiO₂ (P)-C catalysts exhibited superiorities of higher electrochemical surface area, higher level of CO-tolerance, much better activity for formic acid electro-catalytic electrochemical oxidation over Pd/TiO₂-C. The results demonstrated that the self-assembly of Pd NPs onto PDDA-functionalized TiO₂ is an effective and promising method for obtaining catalysts with good dispersion and high stability.

ACKNOWLEDGEMENT

The research was supported by the Hunan Provincial Natural Science Foundation of China (13JJ5018) and the Key Technology R&D Program of Hunan Provincial Science & Technology Department (2009FJ3138)

References

1. C. Rice, S. Ha, R. I. Masel, P. Waszczuk, A. Wieckowski, T. Barnard, *J. Power. Sources*, 111 (2002) 83.
2. S.Y. Wang, N. Kristian, S. P. Jiang, X. Wang, *Electrochem. Commun.*, 10 (2008) 961.
3. X. Yu, P. G. Pickup, *J. Power. Sources*, 182 (2008) 124.
4. C. Rice, S. Ha, R. I. Masel, A. Wieckowski, *J. Power. Sources*, 115 (2003) 229.
5. Y. Zhu, Z. Khan, R. I. Masel, *J. Power. Sources*, 139 (2005) 15.
6. M. N. Nadagouda, V. Polshettiwar, R. S. Varma, *J. Mater. Chem.*, 19 (2009) 2026.
7. C. Hu, X. Zhang, X. S. Li, Y. Yan, G. C. Xi, H. F. Yang, H. Bai, *Chem. Eur. J.*, 20 (2014) 1.
8. Q. Z. Dong, Y. N. Li, L. Y. Zhu, T. Ma, C. C. Guo, *Int. J. Electrochem. Sci.*, 8 (2013) 8191.
9. Q. Z. Dong, L. Y. Zhu, H. S. Wan, C. C. Guo, G. Yu, *Int. J. Electrochem. Sci.*, 9 (2014) 8024.
10. Q. Z. Dong, L. L. Li, Q. S. Chen, C. C. Guo, G. Yu, *Russ. J. Phys. Chem. A.*, 89 (2015) 1452.
11. S. Z. Hu, L. Scudiero, S. Ha, *Electrochim. Acta.*, 83 (2012) 354.
12. S. Sharma, B. G. Pollet, *J. Power. Sources*, 208 (2012) 96.
13. Y. J. Wang, D. P. Wilkinson, J. Zhang. *Chem. Rev.*, 111 (2011) 7625.
14. E. Antolini, *Appl. Catal. B: Environ.*, 88 (2009) 1.
15. J. P. Meyers, R. M. Darling. *J. Electrochem. Soc.*, 153 (2006) A1432.
16. L. M. Roen, C. H. Paik, T. D. Jarvi, *Electrochem. Solid. St.*, 7 (2004) A19.
17. S. Y. Huang, P. Ganesan, S. Park, B. N. Popov, *J. Am. Chem. Soc.*, 131 (2009) 13898.
18. X. L. Cao, Q. X. Li, Y. F. Yao, Q. J. Xu, *Adv. Mater. Res.*, 860 (2014) 812.
19. H. S. Wan, Q. Z. Dong, G. M. Zhu, G. Yu, T. W. Yin, M. L. Huang, *Int. J. Hydrogen Energ.*, 40 (2015) 14179.
20. S. Y. Wang, X. Wang, S. P. Jiang, *Phys. Chem. Chem. Phys.*, 13 (2011) 6883.
21. S. Zhang, Y. Shao, G. Yin, Y. Lin, *Appl. Catal. B: Environ.*, 102 (2011) 372.

22. S. Y. Wang, S. P. Jiang, X. Wang, *Nanotechnology*, 19 (2008) 265601.
23. S. Zhang, Y. Shao, G. Yin, Y. Lin, *J. Mater.Chem.*, 19 (2009) 7995.
24. S.Y. Wang, A. Manthiram, *Electrochim.Acta*, 88 (2013) 565.
25. X. M. Wang, Y. Y. Xia, *Electrochim.Acta*, 55 (2010) 851.
26. L. Manna, E. C. Scher, A. P. Alivisatos, *J. Am. Chem. Soc.*, 122 (2000) 12700.
27. Z. Liu, L. Hong, M. P. Tham, T. H. Lim, H. Jiang. *J. Power. Sources*, 161 (2006) 831.
28. J. Ge, W. Xing, X. Xue, C. Liu, T. Lu, J. Liao, *J. Phys.Chem.C.*, 111 (2007) 17305.
29. R. Wang, S. Liao, S. Ji, *J. Power. Sources*, 180 (2008) 205.
30. D. Morales-Acosta, J. Ledesma-Garcia, L.A. Godinez,, H. G. Rodríguez, L. Alvarez-Contreras, L. G. Arriaga, *J. Power. Sources*, 195 (2010) 461.
31. S. Wang, S. P. Jiang, T. J. White, X. Wang, *Electrochim. Acta*, 55 (2010) 7652.
32. L. Zhang, T. Lu, J. Bao, Y. Tang, C. Li. *Electrochem. Commun.*, 8 (2006) 1625.
33. Z. L. Liu, L. Hong, M. P. Tham, T. H. Lim, H. X. Jiang. *J. Power. Sources*, 161 (2006) 831.
34. M. Marinsek, M. Sala, B. Jancar, *J. Power. Sources*, 235 (2013) 111.
35. A. B. A. A. Nassr, A. Quetschke, E. Koslowski, M. Bron, *Electrochim. Acta*, 102 (2013) 202.
36. G. Zhang, Y. Wang, X. Wang, Y. Chen, Y. Zhou, Y. Tang, L. Lu, J. Bao, T. Lu, *Appl. Catal. B: Environ.*, 102 (2011) 614.
37. S. Yang, C. Shen, X. Lu, H. Tong, J. Zhu, X. Zhang, H. J. Gao, *Electrochim. Acta*, 62 (2012) 242.

© 2016 The Authors. Published by ESG (www.electrochemsci.org). This article is an open access article distributed under the terms and conditions of the Creative Commons Attribution license (<http://creativecommons.org/licenses/by/4.0/>).